

**SYGMA: Stellar Yields for Galactic Modeling Applications**C. Ritter<sup>1,2,6,7</sup>, B. Côté<sup>1,3,4,6,7</sup>, F. Herwig<sup>1,6,7</sup>, J. F. Navarro<sup>1</sup>, C. Fryer<sup>5,7</sup>

critter@uvic.ca

**ABSTRACT**

The stellar yields for galactic modeling applications (SYGMA) code is an open-source module that models the chemical ejecta and feedback of simple stellar populations (SSPs). It is intended for use in hydrodynamical simulations and semi-analytic models of galactic chemical evolution. The module includes the enrichment from asymptotic giant branch (AGB) stars, massive stars, SNIa and neutron-star mergers. An extensive and extendable stellar yields library includes the NuGrid yields with all elements and many isotopes up to Bi. Stellar feedback from mechanics and frequency-dependent radiative luminosities are computed based on NuGrid stellar models and their synthetic spectra. The module further allows for customizable initial-mass functions and supernova Ia (SNIa) delay-time distributions to calculate time-dependent ejecta based on stellar yield input. A variety of r-process sites can be included. A comparison of SSP ejecta based on NuGrid yields with those from Portinari et al. (1998) and Marigo (2001a) reveals up to a factor of 3.5 and 4.8 less C and N enrichment from AGB stars at low metallicity, a result we attribute to NuGrid's modeling of hot-bottom burning. Different core-collapse supernova explosion and fallback prescriptions may lead to substantial variations for the accumulated ejecta of C, O and Si in the first  $10^7$  yr at  $Z = 0.001$ . An online interface of the open-source SYGMA module enables interactive simulations, analysis and data extraction of the evolution of all species formed by the evolution of simple stellar populations.

*Subject headings:* Chemical evolution, stars, nucleosynthesis

---

<sup>1</sup>Department of Physics and Astronomy, University of Victoria, Victoria, BC, V8P5C2, Canada

<sup>2</sup>Keele University, Keele, Staffordshire ST5 5BG, United Kingdom

<sup>3</sup>National Superconducting Cyclotron Laboratory, Michigan State University, MI, 48823, USA

<sup>4</sup>Konkoly Observatory, Research Centre for Astronomy and Earth Sciences, Hungarian Academy of Sciences, Konkoly Thege Miklos ut 15-17, H-1121 Budapest, Hungary

<sup>5</sup>Computational Physics and Methods (CCS-2), LANL, Los Alamos, NM, 87545, USA

<sup>6</sup>JINA-CEE, Michigan State University, East Lansing, MI, 48823, USA

<sup>7</sup>NuGrid collaboration, <http://www.nugridstars.org>

## 1. Introduction

As stars form and evolve, they engulf, process, and lock part of the interstellar medium (ISM) of a galaxy. They also return to the ISM enriched material (‘yields’) in the form of stellar winds and supernovae. This material is recursively processed in further subsequent generation of stars to leave behind an imprint of the enrichment history in the abundance patterns of different stellar populations and in the enriched ISM. The interpretation of these observed patterns thus requires the application of galactic chemical evolution (GCE) models, a field that has developed steadily for the past 4 decades (see, e.g., Audouze & Tinsley 1976; Arnett 1996).

A crucial component of GCE models is the time-dependent element-by-element output returned by evolving stars formed at a given time and at a particular location out of a homogeneously mixed ISM. These are the yields of a simple stellar population (SSP), and include material processed by a range of sources: low-mass stars, massive star winds, supernovae, and merger events that eject elements. The yields of these sources can vary with metallicity. Coupling SSP yields with a time-dependent star formation rate and prescriptions for mixing, accretion, and outflows, a GCE model can evolve the composition of a galaxy (or at least a location, or ‘zone’). The model requires a number of inputs and assumptions, including an initial mass function (IMF), stellar lifetimes, wind mass-loss histories, and merger timescales.

In this paper, we present a open-source module to compute time-dependent SSP yield sets designed for use in GCE models and numerical hydrodynamic simulations. This Stellar Yield for Galactic Modeling Applications (SYGMA) module implements easily-modifiable prescriptions for the IMF, stellar lifetimes, wind mass-loss histories and merger timescales and can be used in a stand-alone manner to assess the impact of stellar evolution model assumptions. SYGMA improves on current SSP yield sets by using the latest NuGrid yield sets (Pignatari et al. 2016; Ritter et al. 2017b), rather than assembling various compilations produced with different stellar evolution codes, post-processing codes and nuclear-physics input. The latter can lead to large uncertainties in yields, as shown in Gibson (2002) and Romano et al. (2010). Indeed, Wiersma et al. (2009, W09) developed a chemical feedback module for hydrodynamic simulations, and found that their SSP ejecta can differ by a factor of two or more for different yields available in literature.

By incorporating the NuGrid yield set, SYGMA provides a consistent set of yields, with the exception of the SNIa and r-process yields. This module is the basic building block of NuGrid’s open-source python chemical evolution framework NuPyCEE and includes examples and analysis tools. SYGMA has been used via NuGrid’s OMEGA code (Côté et al. 2016, 2017b,c,d,e; Ritter et al. 2017a).

Aside from enriching the ISM, stars also alter the surrounding medium through winds and radiation. These energy inputs into the ISM are the basis of the stellar ‘feedback’ introduced in most galaxy simulation codes. A common approach is to adopt feedback prescriptions that neglect any dependence on the stellar models from which the yields were derived. W09, for example, adopt a constant kinetic energy of  $10^{51}$  erg for stars above the zero-age main-sequence mass of  $M_{\text{ZAMS}} = 6 M_{\odot}$ . The SYGMA implements these energy sources based on the stellar models and supernova explosions from the NuGrid data set.

We present the functionality of our code in Sect. 2. In Sect. 3 we analyze the ejecta of SSPs at solar

metallicity and low metallicity based on the new NuGrid yields (Pignatari et al. 2016; Ritter et al. 2017b) compared to the combined yield set of AGB yields of Marigo (2001a, M01) and massive star yields of Portinari et al. (1998, P98). We compare the result of the evolution of key elements ejected by SSP’s presented in W09 by applying their yield set in Sect. 4. Also discussed are the effects of core-collapse mass-cut prescriptions on yields from massive star models. In Sect. 5 we summarize our results.

## 2. Methods

In this section we discuss the physics assumptions and the code implementation. Then we present the details of the stellar yields of our yield library.

### 2.1. Simple stellar population mechanics

A simple stellar population consist of stars formed out of a gas cloud of a certain initial composition in one burst. To follow the gas enrichment of a SSP it is sufficient to track only the ejecta of stars since all initial gas is, by assumption, locked up in stars during the star formation. The composition of the stellar ejecta is based on the yields of stellar models. The latter are calculated with the initial abundance which is the composition of the initial star-forming gas cloud of the SSP. Stellar yields, the total mass of the gas cloud and chemical evolution assumptions determine the total number of stars formed and the total amount of stellar ejecta. Chemical evolution assumptions describe properties of the stellar population such as the number of stars formed in a initial mass range. The chemical evolution assumptions together with the initial mass and metallicity of the gas cloud and stellar yields are required for SSP modeling and determine the chemical enrichment.

In the following the basic assumptions of our simple stellar population model are introduced. Results in this section are based on NuGrid stellar yield input and stellar models (Ritter et al. 2017b), SNIa yields from Thielemann et al. (1986) and NS merger yields from Rosswog et al. (2014). SYGMA of NuPyCEE version 2.5 is used in this work.

#### 2.1.1. Simple stellar population ejecta

SYGMA models the enrichment by AGB stars, massive stars, SNIa and NS mergers. The cumulative contributions from AGB stars, massive stars and SNIa are tracked separately as shown for a SSP of  $10^6 M_{\odot}$  at  $Z = 0.02$  in Fig. 1. Initially, massive stars are the only contributor to the total ejecta due to their short lifetime. Later AGB stars and SNIa start ejecting matter and AGB stars become the dominant source of ejecta.

SYGMA provides analytic tools to identify the most relevant nuclear production site for a given element or isotope. For the SSP of  $10^6 M_{\odot}$  at  $Z = 0.02$  we verify that AGB stars are important producer of C (e.g

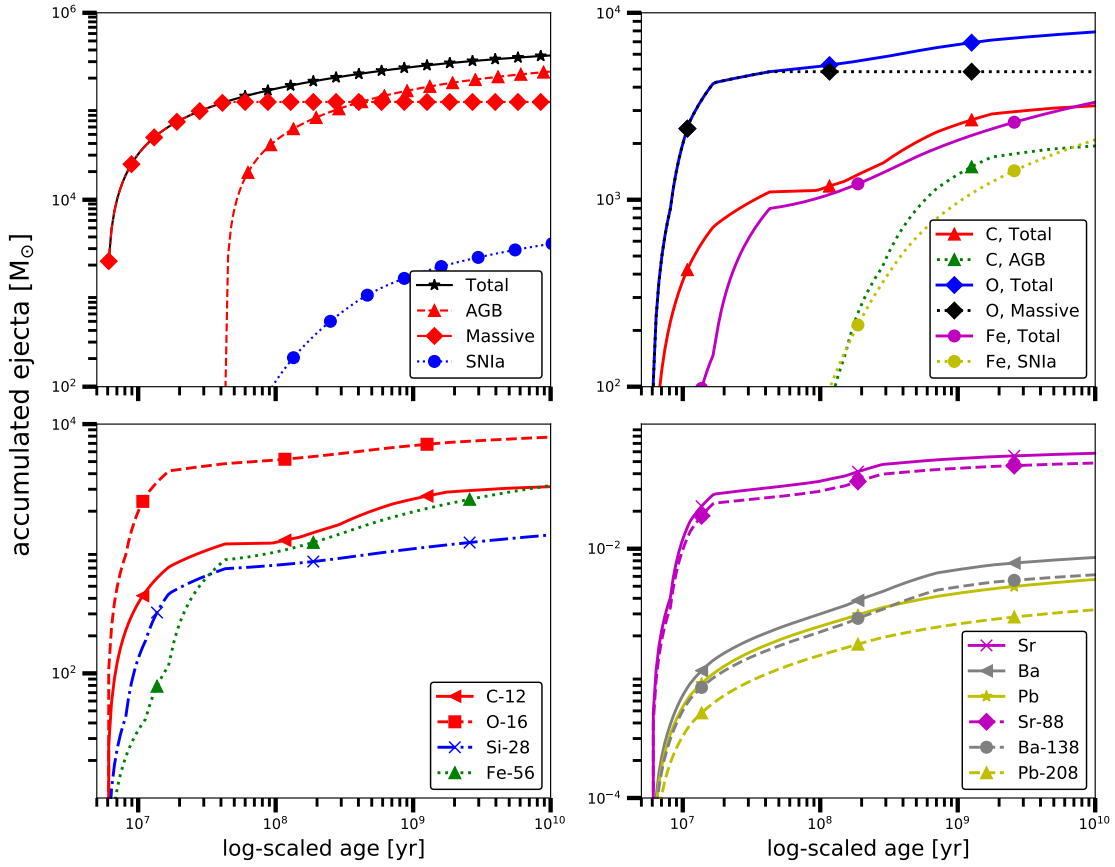


Fig. 1.— Accumulated ejecta from AGB stars, massive stars and SNIa for a SSP of  $10^6 M_{\odot}$  at  $Z = 0.02$  (top, left). Accumulated ejecta of C, O and Fe from all (total) or from distinct sources (top, right). Ejecta from of abundant isotopes of C, O, Si and Fe (bottom, left). Total accumulated ejecta of isotopes and elements of intermediate mass and from the first, second and third s-process peak (bottom, right). Access and interactive exploration of the figures is possible with the WENDI interface (Appendix A).

Schneider et al. 2014) with about 64% of the total amount of C produced (Fig. 1). Massive stars are assumed to produce the most O (e.g Woosley et al. 2002) and we find that 62% of all O originates from massive stars. SNIa produce 63% of the total amount of Fe and are the main source of Fe as found previously (e.g Thielemann et al. 1986). SYGMA tracks all the stable elements and most isotopes up to Bi, as demonstrated for intermediate and heavy elements in Fig. 1. To model the element enrichment through other sources such as r-process from neutrino-driven winds additional yields can be included. These yields are specified as an extra yield table input.

SYGMA adopts the delayed production approximation which is the assumption that all stellar yields are ejected instantaneously after a span corresponding to the stellar lifetime (Pagel 2009). These time spans are provided with the NuGrid yield tables. For AGB models they are the stellar lifetimes until the end of the computation during the thermal-pulse AGB stage or until the end of the post-AGB stage. For massive star models the time span is the time until core collapse. The time span or lifetime  $\tau$  for a certain initial mass  $M$  is derived through a log-log spline fit of the tabulated lifetimes and initial masses (Fig. 2). The mass  $\Delta M_{\text{SSP}}$

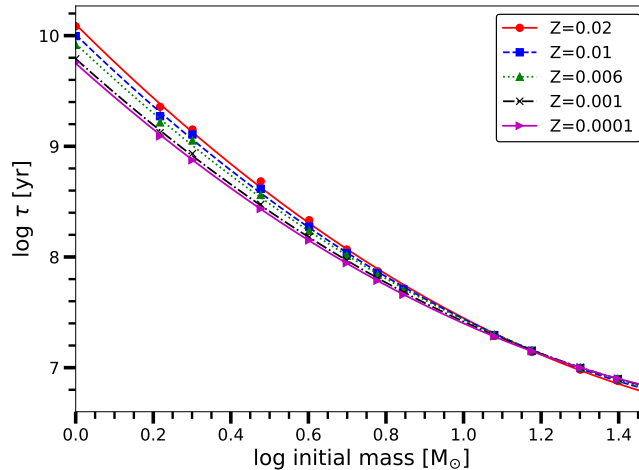


Fig. 2.— Stellar lifetimes  $\tau$  for initial masses of the NuGrid model grid. The fits of the lifetimes over the initial mass range are provided for each metallicity.

lost by a SSP over the time interval  $[t, t+\Delta t]$  is

$$\Delta M_{\text{SSP}} = \int_t^{t+\Delta t} \xi(M_\tau(t')) M_\star(M_\tau(t'), Z) dt' \quad (1)$$

where  $M_\tau(t)$  is the inverse of the lifetime function  $\tau(M)$ .  $\xi(M)$  is the initial mass function normalized to the total gas mass of the SSP and  $M_\star(M, Z)$  is the total ejected mass of the star of mass  $M$  and metallicity  $Z$ . In our 1-zone closed-box approximation the stellar ejecta is homogeneously mixed with the available gas.

### 2.1.2. Initial mass function

The initial mass function  $\xi$  gives the number of stars  $N$  within an initial mass interval  $[m_1, m_2]$  via

$$N = A \int_{m_1}^{m_2} \xi(m') dm' \quad (2)$$

where the normalization constant  $A$  is derived from the total gas mass. SYGMA provides the Salpeter IMF (Salpeter 1955) given as

$$\xi(m) = A_S m^{-\alpha} \quad (3)$$

where  $\alpha = 2.35$ . A single power law with an exponent  $\alpha$  of choice can also be selected. In addition SYGMA provides the Chabrier IMF (Chabrier 2003) which is defined as

$$\begin{aligned} \xi(m) &= A_C m^{-1} e^{-\frac{(\log m - \log m_c)^2}{2\sigma^2}} & \text{for } m \leq 1 M_\odot, \\ \xi(m) &= A_C m^{-2.3} & \text{for } m > 1 M_\odot, \end{aligned} \quad (4)$$

where  $m_c = 0.079$  and  $\sigma = 0.69$ . The Kroupa IMF (Kroupa 2001) is provided as well and calculated as

$$\begin{aligned} \xi(m) &= A_K m^{-0.3} & \text{for } 0.01 M_\odot \leq m \leq 0.08 M_\odot, \\ \xi(m) &= A_K m^{-1.3} & \text{for } 0.08 M_\odot \leq m \leq 0.50 M_\odot, \\ \xi(m) &= A_K m^{-2.3} & \text{for } m \geq 0.50 M_\odot. \end{aligned} \quad (5)$$

These IMF types are discussed in more in detail in Kroupa et al. (2013). Finally, custom IMF can be defined and applied in the code and in the online version. The lower and upper boundaries of the IMF can be set and are related to the onset of H-burning and the occurrence of the most massive stars respectively (see discussion in Côté et al. 2016).

### 2.1.3. Supernova Ia rates

The number of SNe Ia  $N_{\text{Ia}}$  per  $M_\odot$  in the time interval  $[t, t+\Delta t]$  is given by

$$N_{\text{Ia}} = A_{\text{Ia}} \int_t^{t+\Delta t} f_{\text{WD}}(t') \Psi_{\text{Ia}}(t') dt' \quad (6)$$

where  $A_{\text{Ia}}$  is the normalization constant,  $f_{\text{WD}}(t)$  the fraction of white dwarfs and  $\Psi_{\text{Ia}}(t)$  the delay-time distribution (DTD) at time  $t$  (W09). In SYGMA only white dwarfs with initial masses between  $3 M_\odot$  and  $8 M_\odot$  are potential SNIa progenitors as commonly adopted (e.g. Dahlen et al. 2004; Mannucci et al. 2006, W09). The boundaries approximate the lowest mass of a CO white dwarf which can form in a binary system and the maximum white dwarf mass (Yungelson 2005). Either  $A_{\text{Ia}}$  or the total number of SNe Ia per  $M_\odot$  are required as an input. The power-law DTD of Maoz & Mannucci (2012) given as

$$\Psi_{\text{Ia}}(t) = t^{-1} \quad (7)$$

can be selected. The power-law exponent is separately adjustable. We provide an exponential DTD in the form of

$$\Psi_{Ia}(t) = \frac{e^{-t/\tau_{Ia}}}{\tau_{Ia}} \quad (8)$$

and a Gaussian DTD as

$$\Psi_{Ia}(t) = \frac{1}{\sqrt{2\pi}\sigma^2} e^{-\frac{(t-\tau_{Ia})^2}{2\sigma^2}} \quad (9)$$

as in W09.  $\tau_{Ia}$  is the characteristic delay time and  $\sigma$  defines the width of the Gaussian distribution. For a discussion of the parameters see W09 and references within.

#### 2.1.4. Neutron star merger rates

The number of NS mergers  $N_{\text{NS}}$  in the time interval  $[t, t+\Delta t]$  is given as

$$N_{\text{NS}} = A_{\text{NS}} \int_t^{t+\Delta t} \Psi_{\text{NS}}(t', Z) dt' \quad (10)$$

where  $A_{\text{NS}}$  is the normalization constant and  $\Psi_{\text{NS}}(t, Z)$  is the NS DTD. The user can choose between a power law DTD, the DTD of Dominik et al. (2012), or a constant coalescence time. For the DTD based on Dominik et al. (2012) we adopt for the metallicity of  $Z \geq 0.019$  their DTD at solar metallicity and for  $Z \leq 0.002$  their DTD at a tenth of solar metallicity. We interpolate the distribution between these two metallicity boundaries. The normalization constant  $A_{\text{NS}}$  is derived from the total number of merger systems  $N_{\text{NS,tot}}$  via

$$A_{\text{NS}} = \frac{N_{\text{NS,tot}}}{\int \Psi_{\text{NS}}(t, Z) dt'} \quad (11)$$

$N_{\text{NS,tot}}$  is calculated as

$$N_{\text{NS,tot}} = 0.5 f_m f_b \int_{m_1}^{m_2} \xi(m') dm' \quad (12)$$

where  $f_m$  is the fraction of merger of massive-star binary systems and  $f_b$  is the binary fraction of all massive stars.  $f_m$  and  $f_b$  as well as the initial mass range for potential merger progenitors  $[m_1, m_2]$  need to be provided as an input. As an alternative to normalizing the number of NS merger with Eq. (10) the user can directly normalize the rate by providing the total number of NS merger per  $M_{\odot}$  as an input.

#### 2.1.5. Yield implementation

The total yields  $y_{\text{tot},i}$  are defined as the total mass of element/isotope  $i$  ejected over the lifetime of the star and given as

$$y_{\text{tot},i} = y_{0,i} + y_{n,i} \quad (13)$$

where  $y_{0,i}$  refers to the mass of element/isotope  $i$  initially available in the stellar simulation. The net yields  $y_{n,i}$  is the produced or destroyed mass of element/isotope  $i$ . Yield tables with total yields are the default input for SYGMA.

With the application of total yields the assumption holds that the initial abundance of the underlying stellar model  $y_{0,i}$  represents the gas composition of the chemical evolution simulation  $y_{0,\text{sim},i}$  at the time of star formation. If material is unprocessed throughout stellar evolution the total ejecta is  $y_{\text{tot},i} = y_{0,i}$  and the error  $\epsilon_i = y_{0,\text{sim},i} - y_{0,i}$  propagates into the total ejecta. This could lead with  $\epsilon_j > 0$  to the artificial production of the r-process isotope  $j$  if it is based solely on the solar-scaled initial abundance. For element/isotope  $k$  of secondary nucleosynthesis origin  $y_{n,k}$  depends strongly on  $y_{0,k}$  and on the error  $|\epsilon_k|$ .

Net yields can be applied in the code to take into account  $y_{0,\text{sim},i}$  and SYGMA calculates the total ejecta  $y_{\text{tot},i}$  as

$$y_{\text{tot},i} = y_{0,\text{sim},i} + y_{n,i}. \quad (14)$$

With the destruction of element/isotope  $h$  ( $y_{n,h} < 0$ ) and  $\epsilon_h < 0$  more of element/isotope  $h$  is destroyed than initially available and the error is  $|\epsilon_h|$ . In this case the code sets  $y_{\text{tot},h} = 0$ . For the comparison with W09 (Sec. 4) we apply tabulated net yields.

An initial mass interval in which yields are applied can be specified to take into account material locked away in low-mass stars or in massive stars through black hole formation. This IMF yield range goes by default from  $M_{\text{ZAMS}} = 1 M_{\odot}$  to  $M_{\text{ZAMS}} = 30 M_{\odot}$ . The IMF yield range and the IMF range can both be set separately for stars of  $Z > 0$  and Pop III stars to take into account different types of star formation. The yields of a specific tabulated stellar model are applied in an initial mass interval with boundaries given as half the distance to the next available tabulated entries of lower and higher initial mass. If these entries are either not available or outside of the IMF yield range the boundaries of the IMF yield range are applied. The total stellar ejecta  $y_{\text{tot},i}$  for a given initial mass and element/isotope  $i$  is derived from linear fits of the nearest  $y_{\text{tot},i}$  provided in the yield input. Only total yields can be used as SNIa yields input.

### 2.1.6. *Stellar feedback*

Mass ejection rates, stellar luminosities of different energy bands and kinetic energies of SN of SSPs can be modeled with additional input tables. In this section the models are discussed in more detail.

#### **Stellar winds**

The properties of stellar winds are of importance since these winds can contribute to galactic winds which distribute metals and enrich the intergalactic medium (Hopkins et al. 2012). We provide the time evolution of the mass ejection rates of AGB and massive star models of NuGrid as an input for SYGMA. The mass loss rates for a SSP of  $10^6 M_{\odot}$  at solar metallicity (Fig. 3) decrease with time due to the declining AGB mass loss rates towards lower initial masses and are similar Fig. 3 and Fig. 4 in Côté et al. (2015). The steps in the evolution of the ejected mass origin from the transition between grid points of the stellar model grid. The strongest AGB mass loss originates from the  $5 M_{\odot}$  stellar model as visible in the peak shortly after  $10^8$  yr. To determine the kinetic energy of stellar winds  $E_{\text{wind}}$  we calculate for each stellar model the

time-dependent escape velocity  $v_{\text{esc}}$  via

$$v_{\text{esc}}(t) = \sqrt{\frac{2GM(t)}{R(t)}} \quad (15)$$

where  $M(t)$  and  $R(t)$  are the total mass and radius of a stellar model at time  $t$ .

After deriving the terminal velocity  $v_{\infty}$  from  $v_{\text{esc}}$  one can calculate the kinetic energy as

$$E_{\text{wind}}(t) = \frac{1}{2} \dot{m}(t) v_{\infty}(t)^2. \quad (16)$$

Abbott (1978) found the relation  $v_{\infty} = 3v_{\text{esc}}$  for observed O, B, A and Wolf-Rayet stars via radiation-driven wind theory. We apply this relation because  $E_{\text{wind}}$  dominantly origins from the most massive stars with radiative winds (Leitherer et al. 1992).

The stellar grid includes stellar models up to  $M_{\text{ZAMS}} = 25 M_{\odot}$  while stellar models at higher initial mass are expected to contribute the majority of the kinetic wind energy of the stellar population. Hence our kinetic energy of winds are similar to those of the SSP with upper IMF limit of  $30 M_{\odot}$  of `starburst99` (Fig. 111, Leitherer et al. 1999).

For AGB models we approximate  $v_{\infty}$  as  $v_{\infty} = v_{\text{esc}}$  which might overestimate the kinetic energy contribution of the AGB phase as indicated by observations (Bolton 2000). Energetic contributions of AGB stars are often not considered in SSP models since their contribution is negligible compared to massive stars (Leitherer et al. 1999; Côté et al. 2015). Our largest kinetic energies of winds originate from massive star models while the kinetic energies of winds from AGB models are considerably smaller (Fig. 3).

### Supernova energies

The kinetic energies of CCSNe is canonically taken as  $10^{51}$  erg which is similar to the observed explosion energies of SN such as SN 1987A (Arnett et al. 1989). We apply CCSN energies based on the CCSN explosion prescription of Fryer et al. (2012) used for NuGrid stellar models. For each initial mass and metallicity of the stellar models the kinetic energy is extracted from Fig. 2 of Fryer et al. (2012). Energies for stellar models above  $25 M_{\odot}$  are not taken into account because such stellar models are not included in the NuGrid model grid because they do not explode according to our remnant mass model. The kinetic energy of a SNe Ia is an input parameter of `SYGMA` and is set to  $10^{51}$  erg.

For a SSP of  $10^6 M_{\odot}$  at solar metallicity the kinetic energy from CCSN explosions of  $\approx 10^{40}$  ergs<sup>-1</sup> is similar to `starburst99` (Fig. 113, Leitherer et al. 1999). The kinetic energies from SNe Ia is more than 1 dex lower than the kinetic energy from CCSN explosions (Fig. 3) and very similar to Côté et al. (2015, Fig. 4).

### Stellar luminosities

Stellar radiation alters the surrounding medium through ionization and the momentum flux due of radiation pressure. `SYGMA` computes luminosities of SSPs based on time-dependent bolometric luminosities of stellar models. The latter are provided as table input. The luminosities in specific wavelength bands

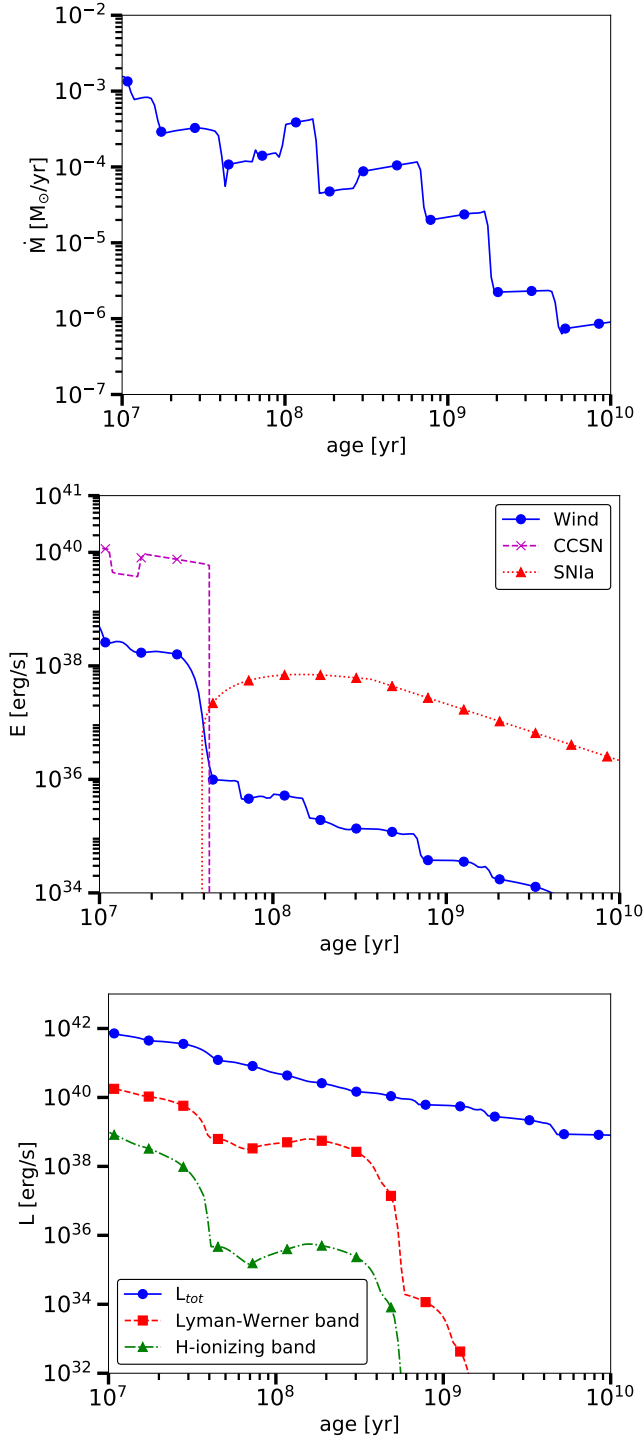


Fig. 3.— Evolution of mass ejection of a SSP of  $10^6 M_{\odot}$  at solar metallicity (top). Kinetic energies of stellar winds, CCSNe and SNe Ia (middle). Time dependence of the total luminosity and luminosities in the Lyman-Werner and H-ionizing bands emitted by the SSP (bottom).

such as the H-ionizing band (13.6 eV - 24.6 eV) are calculated as well as the time-dependent luminosities of luminosity bands based on spectra of the stellar evolution models. The latter are from the PHOENIX (Husser et al. 2013) and ATLAS9 (Castelli & Kurucz 2004) synthetic spectra libraries.

Spectra are derived from the best match of effective temperature  $T_{\text{eff}}$ , the gravity  $g$ ,  $[\text{Fe}/\text{H}]$  and  $\alpha$ -enhancement of a stellar model. We adopt the  $\alpha$ -enhancement of the initial abundance of the stellar models and neglect any changes of the surface abundance during the stellar evolution. The  $\alpha$ -enhancement at low metallicity of NuGrid models is based on observations of individual elements and each element has its own enhancement. The corresponding average  $\alpha$ -enhancement is  $[\alpha/\text{Fe}] = 0.8$  by taking into account the initial abundance of each element. The bolometric luminosity as well as the luminosity in two wavelength bands of a SSP of  $10^6 M_{\odot}$  at  $Z = 0.02$  are shown the lower panel of Fig. 3.

## 2.2. Stellar yields

Metallicities for which stellar yields are provided can be selected as initial metallicities of the SSP. Yields with an arbitrary number of isotopes can be used. The lifetime and final mass for each star are required in the yield input tables. In the following we introduce the yield sets of our comprehensive yield library for SYGMA. Additional yields can be added on request.

The default yields of AGB models, massive star models and core-collapse supernova models are from the NuGrid collaboration and include the metallicities  $Z = 0.02, 0.01, 0.006, 0.001$  and  $0.0001$  (yield sets NuGrid<sub>d/r/m</sub>, Table 1, Ritter et al. 2017b). Yields for twelve stellar models between  $M_{\text{ZAMS}} = 1 M_{\odot}$  and  $M_{\text{ZAMS}} = 25 M_{\odot}$  are provided for each metallicity, including super-AGB models. The TP-AGB stages of

ID	Masses	Metallicity	S-AGB	heavy-element processes	network	exp
NuGrid <sub>d/r/m</sub>	1 - 25	0.0001 - 0.02	yes	main s, weak s, p, $\gamma$	Pb	yes
M01P98	1 - 120	0.0004 - 0.05	no	-	Fe	no
K10K06	1 - 40	0.0001 - 0.02	no	-	Ni	yes
C15K06	1.3 - 40	0.0001 - 0.02	no	main s	Ge	yes

Table 1: Properties of yield sets of AGB and massive stars available in SYGMA. Shown are the NuGrid sets (Pignatari et al. 2016; Ritter et al. 2017b) with delayed (NuGrid<sub>d</sub>), rapid (NuGrid<sub>d/r/m</sub>), and mixed CCSN explosion prescription (NuGrid<sub>m</sub>) as discussed in Sect. 4. In comparison the yield sets M01P98 (Marigo 2001b; Portinari et al. 1998), K10K06 (Kobayashi et al. 2006; Karakas et al. 2010) and C15K06 (Cristallo et al. 2015; Kobayashi et al. 2006). Properties are the initial mass and metallicity range, available S-AGB models, the modeled heavy-element processes, the heaviest available stable element in the network provided and the modeling of the CCSN explosion.

low- and intermediate-mass stars and all burning stages of massive stars until collapse are included. All stable elements and many isotopes up to Bi are provided in the yield tables. Convective boundary mixing is applied at all convection zones in AGB models. A nested-network approach allows to resolve hot-bottom burning during post-processing and predicts isotopes of the CNO cycle and s process isotopes. As part of

the semi-analytic explosion prescription a mass- and metallicity dependent fallback is applied which takes into account the observed NS and BH mass distribution. Fallback in stellar models of high initial mass leads to black hole formation. Yield sets are available for delayed explosions (NuGrid<sub>d</sub>), rapid explosions (NuGrid<sub>r</sub>) and a combination of both (NuGrid<sub>m</sub>, see Sect. 4.2). The NuGrid data is available online as tables and through the WENDI interface (Appendix A).

The yield set of the Padua group (M01P98) consists of AGB yields from M01 and massive star yields from P98. Stellar yields for initial masses between  $M_{\text{ZAMS}} = 1 M_{\odot}$  and  $M_{\text{ZAMS}} = 120 M_{\odot}$  and  $Z = 0.02, 0.008, 0.004, 0.0004$  are available. The AGB stage of stellar models up to  $M_{\text{ZAMS}} = 5 M_{\odot}$  is based on synthetic models which are calibrated against observations. For stellar mass models with  $M_{\text{ZAMS}} = 6 M_{\odot}$  and  $M_{\text{ZAMS}} = 7 M_{\odot}$  the AGB stage is not modeled. The contribution from CCSN nucleosynthesis of the massive star models is derived from the explosions of massive star models of Woosley & Weaver (1995).

AGB yields from Karakas et al. (2010) and massive star yields from Kobayashi et al. (2006) are provided in the yield set K10K06. Yields with initial masses between  $M_{\text{ZAMS}} = 1 M_{\odot}$  and  $M_{\text{ZAMS}} = 40 M_{\odot}$  and for  $Z = 0.02, 0.008, 0.004, 0.001, 0.0001$  are included. AGB yields are available up to  $M_{\text{ZAMS}} = 6 M_{\odot}$ . Stellar yields include elements up to Ni and Ge respectively and we adopt elements up to Ni in the K10K06 yield set. Explosive nucleosynthesis is based on CCSN and hypernova models with a mass cut set to limit the amount of ejected Fe to  $0.07 M_{\odot}$ . Hypernova models adopt a mixing-fallback mechanism which is adjusted so that  $[\text{O}/\text{Fe}] \simeq 0.5$ . For stellar models for which SN and hypernova yields are available we choose a mix of 50% SN yields and 50% hypernova yields as K06.

Yields of light and heavy elements for AGB models up to  $M_{\text{ZAMS}} = 6 M_{\odot}$  are provided in the F.R.U.I.T.Y. database (e.g. Cristallo et al. 2015). We combine F.R.U.I.T.Y. yields with those of K06 in the C15K06 yield set which includes  $Z = 0.02, 0.008, 0.004, 0.001, 0.0001$ . Since yields of K06 are available only until Ge the C15K06 yield set does not include the heavier elements provided in the F.R.U.I.T.Y. database.

Additional yield sets can be created through combination of other yield tables. Available options include CCSN yields, hypernova yields and pair-instability supernova yields of Nomoto et al. (2013). Zero-metallicity massive star yields are from Heger & Woosley (2010). Yields of magneto-hydrodynamic explosions of massive star models are from Nishimura et al. (2015). CCSN neutrino-driven wind yields are based on simple trajectories of analytic models (N. Nishimura, private communication). r-process yields which are calculated with the solar-system residual method are from Arnould et al. (2007). Yield tables of the dynamic ejecta of NS models which reproduce the strong r-process component are from Rosswog et al. (2014).

Yields of 1D SNIa deflagration models are from Thielemann et al. (1986), Iwamoto et al. (1999) and Thielemann et al. (2003). Yields of Seitenzahl et al. (2013) are based on tracer particles of 3D hydrodynamic simulations of delayed-detonation SNIa models and are available for progenitor metallicities of  $Z = 0.02, 0.01, 0.002, 0.0002$ .

### 3. Results

#### 3.1. Simple stellar populations at solar metallicity

We compare the ejecta of two SSPs based on the yield set NuGrid<sub>d</sub> and the yield set M01P98. Applied are NuGrid yields at  $Z = 0.02$ , P98 yields at  $Z = 0.02$  and M01 yields at  $Z = 0.019$  which we will refer to as yields at solar metallicity. As the initial abundance those of the NuGrid yield calculations are selected (Pignatari et al. 2016). We calculate the total yields  $y_{\text{tot}}$  from the net yield set M01P98 (Sec. 2.1.5) and modify massive star yields by the factors 0.5, 2 and 0.5 for C, Mg and Fe as in W09.

Identical SSP parameters (Table 2) allow to analyze only the differences due to M01P98 yields and NuGrid yields. We choose  $M_{\text{mass}}^1$  in agreement with the upper limit of the progenitors of SNIa applied in the SSP code (Sect. 2.1.3). For SSPs of  $10^4 M_{\odot}$  the evolution of the total accumulated mass of AGB stars

IMF type	Chabrier
IMF range	0.1 - 100 $M_{\odot}$
IMF yield range*	1 - 30 $M_{\odot}$
IMF yield range <sup>+</sup>	0.8 - 100 $M_{\odot}$
$\tau_{\text{Ia}}$	$2 \times 10^9$ yr
$A_{\text{Ia}}$	0.02
$M_{\text{mass}}$	8 $M_{\odot}$

Table 2: Chemical evolution parameters of the SSPs applied in this work. For the initial mass range (IMF range) a Chabrier (2003) IMF were selected. IMF ranges for Sect. 3 (\*) and Sect. 4 (+) are shown. The characteristic delay time  $\tau$  and a normalization parameter  $A_{\text{Ia}}$  of the exponential DTD are given.

and massive stars is about the same for NuGrid yields and M01P98 yields due similar amounts of total ejecta of both yield sets.

**C, N** — AGB stars are important dust producer (e.g. Ferrarotti & Gail 2006; Schneider et al. 2014) and feature the primary production of C (Herwig 2005). In massive and super-AGB stars C is transformed into N in hot-bottom burning (HBB) in the TP-AGB stage (Lattanzio et al. 1996). The TP-AGB phase changes dramatically the structure and chemistry of intermediate mass models. Lower C yields in the NuGrid stellar models of  $M_{\text{ZAMS}} = 6 M_{\odot}$  and  $M_{\text{ZAMS}} = 7 M_{\odot}$  compared to stellar models of lower initial mass is due to more efficient  $^{12}\text{C}$  destruction in the CNO cycle during HBB. The stellar models with  $M_{\text{ZAMS}} = 6 M_{\odot}$  and  $M_{\text{ZAMS}} = 7 M_{\odot}$  by P98 do not include the TP-AGB phase, the third dredge-up (TDUP) and destruction of C during HBB. The accumulated ejecta of  $^{12}\text{C}$  of the SSP with M01P98 yields is higher than with NuGrid yields before  $\approx 2 \times 10^8$  yr (Fig. 4).

<sup>1</sup> $M_{\text{mass}}$  is the initial mass which marks the transition from AGB stars to massive stars.

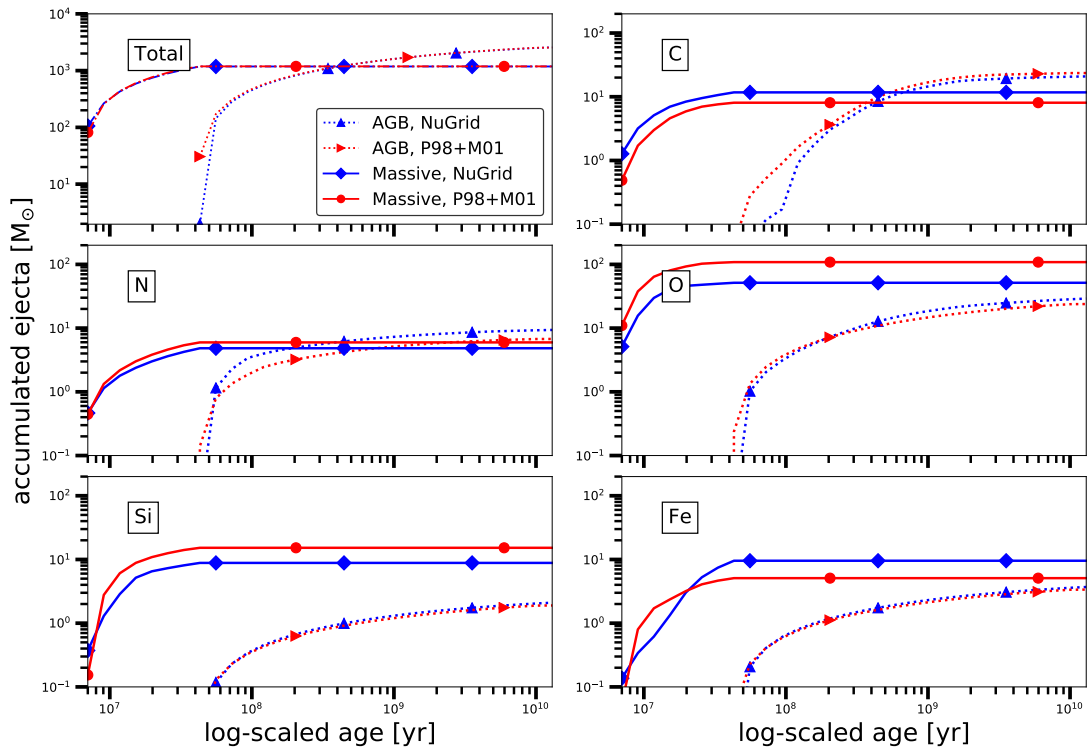


Fig. 4.— Accumulated ejecta of AGB stars and massive stars at solar metallicity based on NuGrid yields and M01P98 yields.

While the total SSP ejecta of C from AGB stars are 11% lower for NuGrid yields than for M01P98 yields, for massive stars total SSP ejecta are 30% larger. The massive stars of the SSP with NuGrid yields produce at all times more C than those of the SSP with M01P98 yields. Without the decrease of massive star yields of P98 by 0.5 as in this work and in W09 M01P98 yields would produce the most C. In the latter case AGB stars would start to dominate the total production of C at  $9 \times 10^8$  yr instead of  $3.6 \times 10^8$  yr.

HBB transforms  $^{12}\text{C}$  into  $^{14}\text{N}$  which leads to larger stellar yields of N from NuGrid compared to stellar models of M01P98 (Fig. 5). The result is a bump in the IMF-weighted ejecta of stellar models with  $M_{\text{ZAMS}} = 6 M_{\odot}$  and  $M_{\text{ZAMS}} = 7 M_{\odot}$ . AGB stars based on NuGrid yields eject in total 28% more N than those with M01P98 yields. For massive stars it is 18% less N with NuGrid yields compared to M01P98 yields.

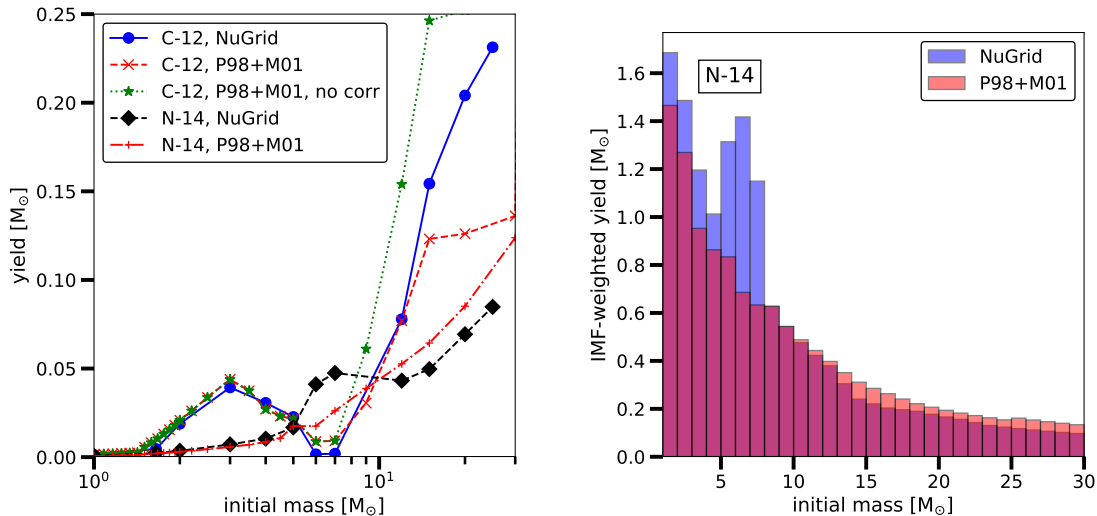


Fig. 5.—  $^{12}\text{C}$  and  $^{14}\text{N}$  yields at solar metallicity versus initial mass of NuGrid, M01P98 and M01P98 without correction factor (no corr) of 0.5 (left). IMF-weighted yields of  $^{14}\text{N}$  of stars of different initial mass (right).

**O, Si** — It is widely accepted that most O is produced in massive stars (Timmes et al. 1995; Woosley et al. 2002). Larger O shells for more massive stars do not necessary lead to larger amounts of O ejected when strong fallback is taken into account. In stellar models with  $M_{\text{ZAMS}} = 20 M_{\odot}$  and  $M_{\text{ZAMS}} = 25 M_{\odot}$  from NuGrid strong fallback of large parts of the O shell results in larger remnant masses and less O ejection at high initial mass compared to P98 (Fig. 6). This results in 47% lower O ejecta of the SSP than compared to the SSP with M01P98 yields (Fig. 6, Fig. 4).

AGB models of NuGrid include convective boundary mixing which results in He-intershell enrichment of O of about 15% in low-mass TP-AGB models compared to 2% without any convective boundary mixing (Herwig 2005). M01 do not include any convective boundary mixing which is why the mass of O from AGB

stars is higher with NuGrid yields than with M01 yields. We find that the effect convective boundary mixing on the total AGB production of O is small as the difference in SSP ejecta between NuGrid yields and M01 yields is only 17% (Fig. 4).

Si is produced in massive stars (e.g. Timmes et al. 1995). Due to its closer proximity to the core than lighter elements we find that the difference in chemical evolution of Si based on NuGrid and M01P98 yields are only slightly smaller than for O. In total 43% less Si is ejected with NuGrid yields than with yields of M01P98. AGB stars eject mostly unprocessed Si and the total amount ejected is within 10% between the yield sets.

**Fe** — The SSP ejecta of Fe of massive stars are qualitatively different between the yield sets (Fig. 4) due to the variation of Fe yields with initial mass (Fig. 6). Most Fe of NuGrid yields comes from massive star models at the lowest initial mass. M01P98 Fe yields are the largest at  $M_{ZAMS} = 20 M_{\odot}$ . Within the first  $2 \times 10^7$  yr the SSP ejecta of Fe from massive stars is up to a factor of three larger for yields of P98 compared to NuGrid yields. At later times the SSP ejecta of Fe from massive stars based on NuGrid yields are larger and the total ejecta based on NuGrid is 47% larger than the one based on M01P98 yields. SSP ejecta of Fe of AGB stars is unprocessed and its total amount ejected is within 10% between yield sets.

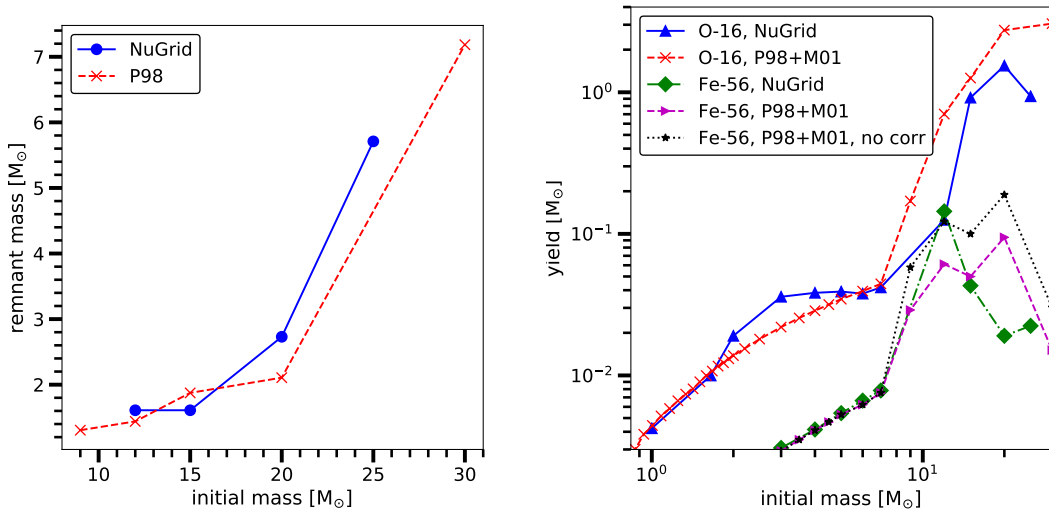


Fig. 6.— Remnant masses versus initial mass of NuGrid and P98 models at solar metallicity (left). Yields of O represented by  $^{16}\text{O}$  and Fe yields represented by  $^{56}\text{Fe}$  at solar metallicity versus initial mass (right).

### 3.2. Simple stellar populations at low metallicity

To analyze the SSP ejecta at low metallicity we compare the yield set NuGrid<sub>d</sub> at  $Z = 0.001$  with the yield set M01P98 at  $Z = 0.004$ . To calculate the total yields from M01P98 net yields (see Sect. 2.1.5) we use

as the initial abundance those adopted for NuGrid models at solar  $Z$  but scaled down to  $Z = 0.004$ . Yields of both sets at the same sub-solar metallicity are not available. The initial abundance of NuGrid yields at  $Z = 0.001$  is  $\alpha$ -enhanced in contrast to P98 and M01. We compare the total accumulated ejecta of AGB stars and massive stars based on yields from M01P98 with those based on NuGrid yields (Fig. 7).

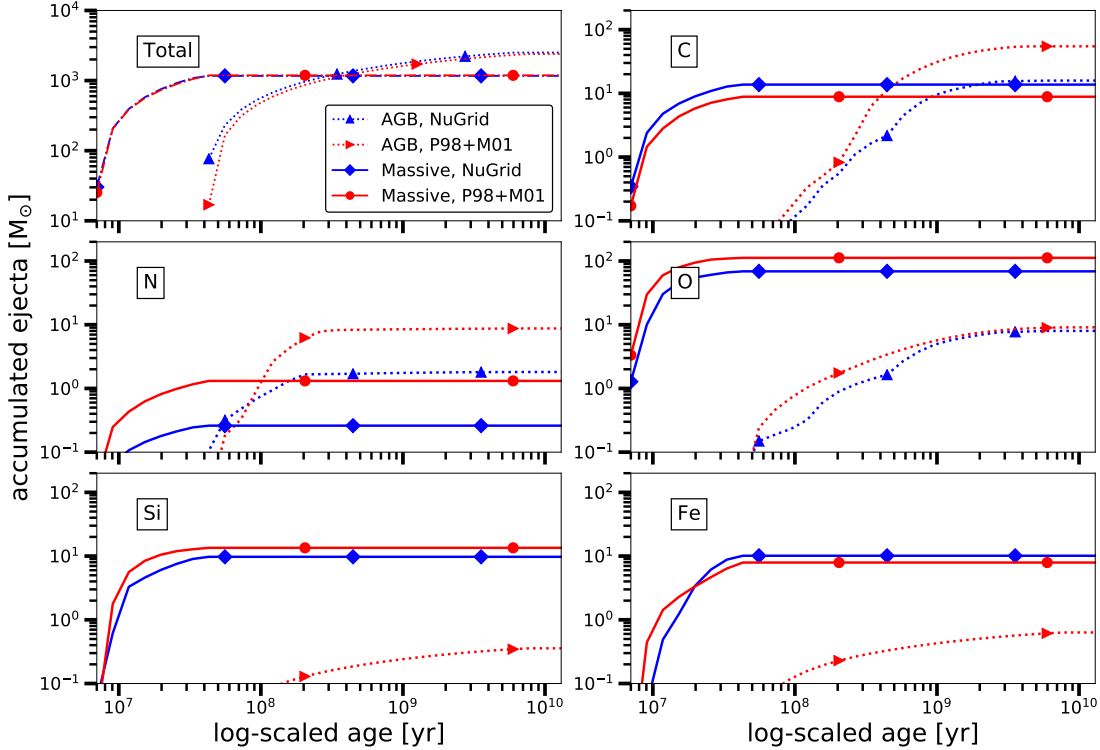


Fig. 7.— Accumulated ejecta of AGB stars and massive stars based on NuGrid yields at  $Z = 0.001$  and M01P98 yields at  $Z = 0.004$ .

**C, N** — The total SSP ejecta of C from AGB stars is 71% lower with NuGrid yields compared to yields of M01P98 (Fig. 7). This is due to the low-mass AGB models of P98 which eject larger amounts of C compared to NuGrid models (Fig. 8). M01 use synthetic models which do not model the TDUP self-consistently contrary to the NuGrid models. In the synthetic models the dredge up of C into the envelope results from the calibration of the dredge-up strength and minimum core mass of TDUP occurrence against the observed carbon star luminosity distribution. The total SSP ejecta of C of massive stars is with NuGrid yields 37% higher than with M01P98 yields.

The total AGB ejecta of N of the SSP based on NuGrid yields is 80% lower than the N ejecta based on

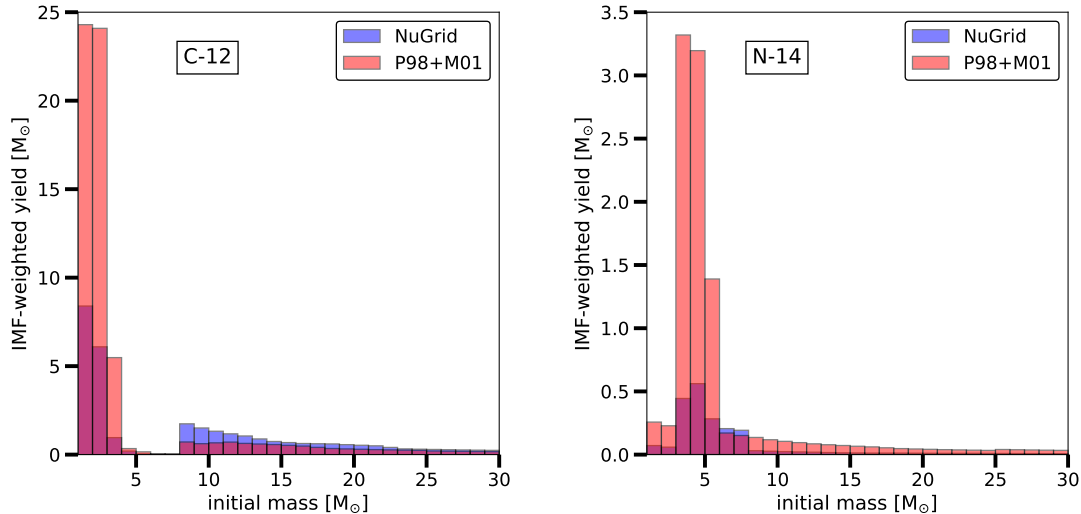


Fig. 8.— IMF-weighted yields of C represented by  $^{12}\text{C}$  and N represented by  $^{14}\text{N}$  versus initial mass based on NuGrid yields with  $Z = 0.001$  and M01P98 yields with  $Z = 0.004$ .

M01P98 yields. We find large discrepancies between N yields from NuGrid and yields of M01 for massive AGB models (Fig. 8). The amounts of N produced in these stellar models during HBB depend on the length of the TP-AGB phase which is based on free parameters of the synthetic models of M01. The SSP ejecta of N of massive stars with NuGrid yields is for most of the evolution 80% lower for than with yields by M01P98.

**O, Si** — The stellar yields of O from AGB models differ more between the yield sets at lower metallicity than at solar metallicity. The difference is the largest for the most massive AGB models. This translates in a large difference of AGB ejecta of the SSPs early on in the evolution (Fig. 7). With NuGrid yields the total amount of O ejected by AGB stars is 12% below the amount ejected with M01P98 yields.

The evolution of SSP ejecta of O from massive stars is in slightly better agreement between the yield sets at low metallicity than at solar metallicity. The total SSP ejecta of O of massive stars with NuGrid yields is 39% lower than with M01P98 yields.

There is little SSP ejecta of Si from AGB stars with M01P98 yields and predictions with NuGrid yields are below the figure boundaries. This Si ejecta discrepancy is due to the initial abundance which differs between yield sets because NuGrid applies an  $\alpha$ -enhanced initial abundance for models of  $Z = 0.001$ . When we apply the same initial abundance of Si AGB ejecta of both sets are in good agreement. The SSP ejecta of Si from massive stars are similar for the yield sets as at solar metallicity. We find a 28% lower total amount of Si ejected by massive stars of NuGrid compared to M01P98.

**Fe** — Fe ejecta from AGB stars based on NuGrid yields are lower than with M01 yields due to the initial abundance and hence below the figure boundary. SSP ejecta of Fe of massive stars based on NuGrid yields starts below and then increases above the ejecta based on M01P98 yields. The strong fallback in NuGrid models of high initial mass limits the Fe ejecta at early times in the SSP evolution. The total amount of Fe ejected is 23% larger with NuGrid yields than with M01P98 yields.

## 4. Discussion

### 4.1. Comparison with Wiersma et al.

In order to verify the SYGMA code we compare the SSP ejecta calculated with SYGMA with the results presented in W09, using the same set of stellar yields as in W09. We apply the net yields of AGB star models by M01 and net yields of massive star models by P98. We modify C, Mg and Fe yields of massive star models by a factor of 0.5, 2 and 0.5 as in W09. The initial abundance of elements is taken from Table 1 of W09. We aim to adopt the same chemical evolution parameter as in that work (Table 2).

The initial mass range for which yields were ejected is not given W09 and we choose the range from  $M_{\text{ZAMS}} = 0.8 M_{\odot}$  to  $M_{\text{ZAMS}} = 100 M_{\odot}$  to match best Fig. 2 in W09. The lower limit is the lowest initial mass of stellar models to ignite central He and to enter the AGB stage (Karakas 2011). Stars of lower initial mass are not of relevance due to their long lifetime beyond the Hubble time.

The choice of  $M_{\text{mass}}$  is not given in W09. It might be in the transition range from the largest intermediate-mass model of  $M_{\text{ZAMS}} = 7 M_{\odot}$  to the smallest massive star model of  $M_{\text{ZAMS}} = 9 M_{\odot}$  of the M01P98 set.  $M_{\text{mass}}$  depends on the upper limit of super-AGB stars and their electron-capture SN channel. Poelarends et al. (2008) estimated  $M_{\text{mass}} = 9.25 M_{\odot}$  based on their models of solar metallicity but the threshold might vary with metallicity (Doherty et al. 2015, 2017).  $M_{\text{mass}}$  depends sensitively on the core growth which in turn depends on the choice of mass loss and efficiency of TDUP in the AGB stage. Jones et al. (2016) found that an increasing convective boundary mixing efficiency increases the TDUP efficiency in super-AGB stars and impedes core growth which would increase  $M_{\text{mass}}$ . Our choice of  $M_{\text{mass}}$  (Table 2) agrees best with the accumulated fraction of ejecta of AGB stars, massive stars and SNe Ia of Fig. 2 in W09.

We compare the accumulated fraction of total ejecta of AGB stars, massive stars and SNe Ia of our SSP model with W09 at solar metallicity (Fig. 9). The uncertainty related to the value of the transition mass  $M_{\text{mass}}$  translates into a uncertainty of the appearance of the AGB star ejecta and the drop in total massive star ejecta as shown for  $M_{\text{mass}} = 7.5 M_{\odot}$ ,  $8 M_{\odot}$  and  $8.5 M_{\odot}$  in Fig. 10.

Our prediction of the evolution of C shows up to 10% less ejecta from intermediate-mass stars compared to W09. There is a better agreement above  $10^9$  yr when stars below  $M_{\text{ZAMS}} = 2 M_{\odot}$  start ejecting their material. The N yields increase smoothly with initial mass which leads to a smooth increase of the SSP ejecta similar to W09. The C and N evolution depends on the yield interpolation in the initial mass transition region from AGB to massive stars. We perform a linear fits of the total ejected yields over the initial mass range (Sect. 2.1.5) while we do not know the treatment in W09. The change of the total ejecta over the initial

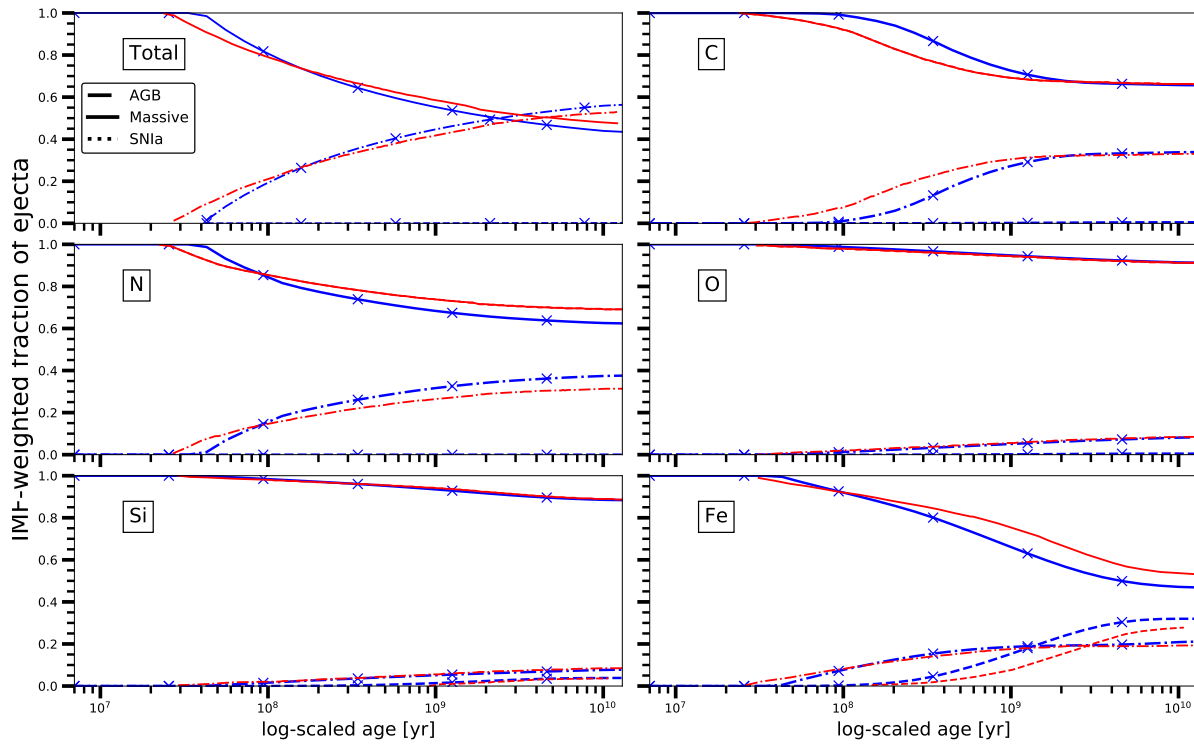


Fig. 9.— Fraction of total mass ejected from AGB, massive star and SNe Ia for a SSP at solar metallicity with yield input from M01P98 (blue, crosses) compared to results extracted from Fig. 2 in W09 (red). Results are based on the same yield input but different SSP codes.

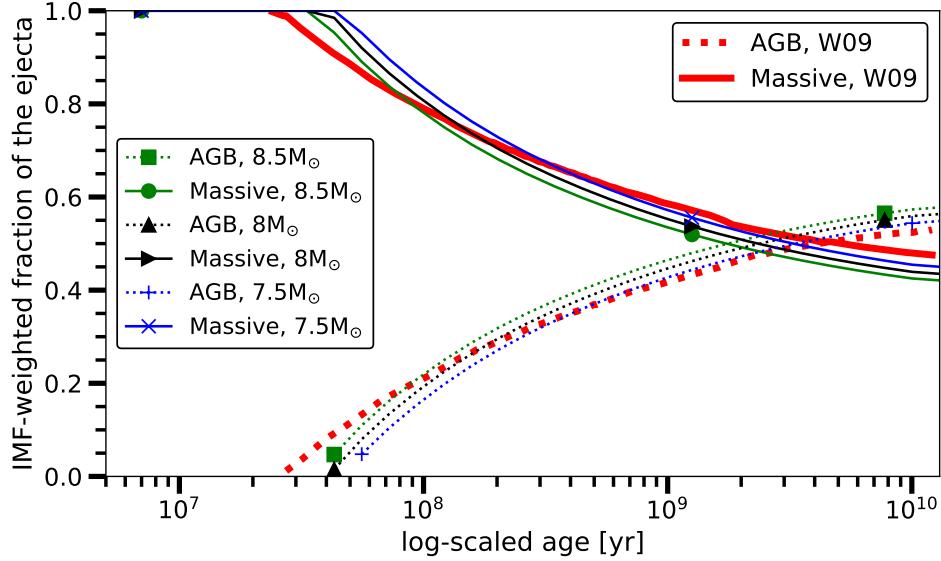


Fig. 10.— Top: Evolution of fraction of total ejecta for transition masses of  $M_{\text{ZAMS}} = 7.5 M_{\odot}$ ,  $M_{\text{ZAMS}} = 8 M_{\odot}$  and  $M_{\text{ZAMS}} = 8.5 M_{\odot}$ .

mass transition region  $M_{\text{mass}}$  between the AGB star model of  $M_{\text{ZAMS}} = 7 M_{\odot}$  and the massive star model at  $M_{\text{ZAMS}} = 9 M_{\odot}$  is shown in Fig. 11. In this region the total ejecta increases by about one third and the stellar

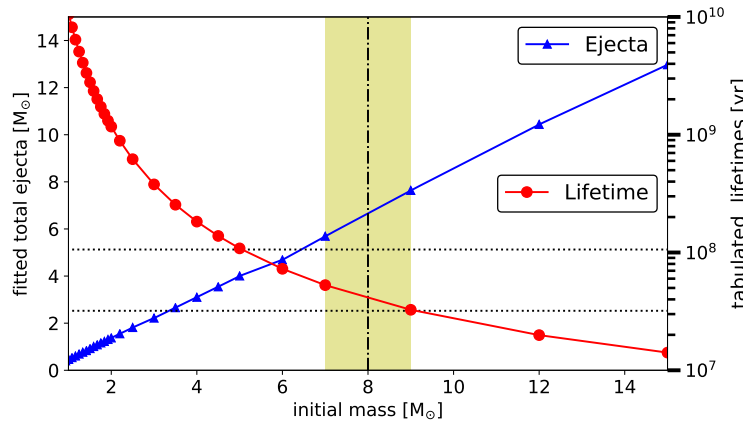


Fig. 11.— Fits of the stellar lifetime and total ejected mass versus initial mass for M01P98. The available initial masses are indicated by the marker. The yellow shaded region indicates the transition from the yield set of M01 to the massive star yields of P98. The dashed-dotted line represents the transition mass of  $M_{\text{mass}} = 8 M_{\odot}$  used in this work.

lifetime decreases by more than 50% towards higher initial mass.

Another uncertainty is the dependence of the stellar ejecta on the initial mass. In SYGMA, yields of a specific stellar model are applied in an initial mass interval given by half the distance to the neighbouring stellar models. Since we do not know about the approach of W09 differences due the yield interpolation methods can be expected. The strong variation of C and N yields of massive AGB models combined with different model assumptions might explain the deviation between our results and W09.

The elements O and Si agree very well with W09 (Fig. 9). They are dominantly produced in massive stars within the first  $3 \times 10^7$  yr and the dependence of the massive star ejecta on initial mass cannot be analyzed through Fig. 9 due to its axis limits. The evolution of Fe ejecta of massive stars and SNe Ia are qualitative similar while the differences are of similar magnitude as for C. The contribution from AGB stars stems from the initial, unprocessed material and there is good agreement between our result and W09.

We compare the evolution of  $[C/Fe]$ ,  $[N/Fe]$ ,  $[O/Fe]$  and  $[Si/Fe]$  with W09 (Fig. 12). The overall largest

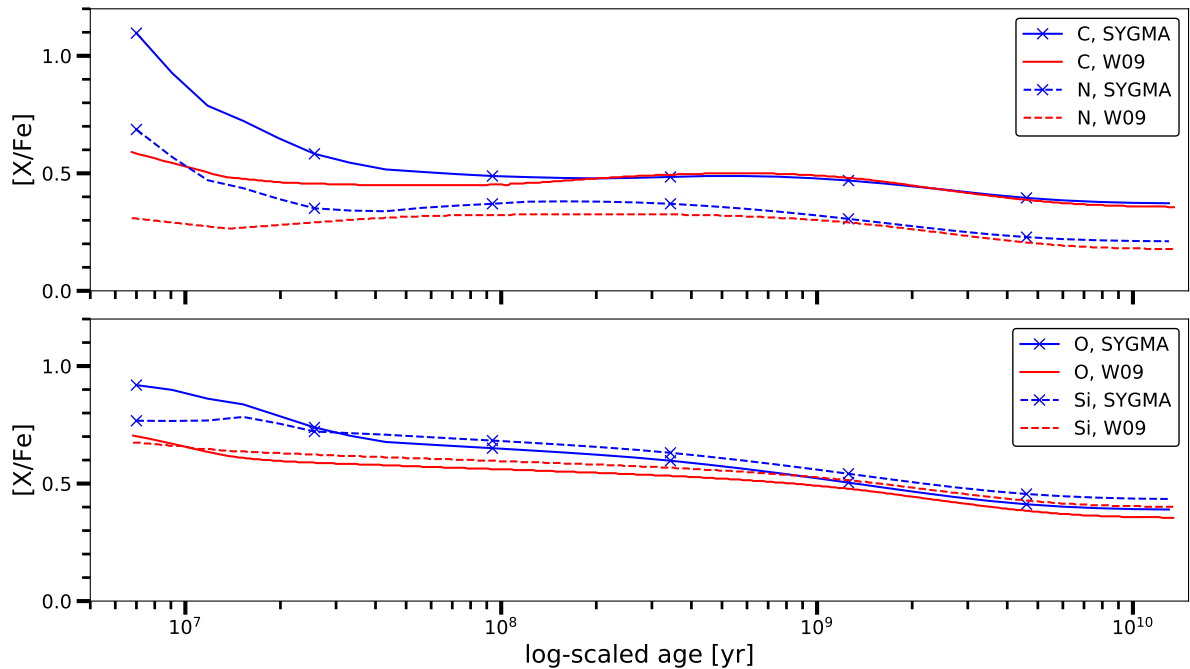


Fig. 12.— Elemental ratios of the total ejecta of a SSP at solar metallicity simulated with SYGMA compared to results by W09. All calculations are with yields from M01P98.

differences are found within the first  $\approx 2 \times 10^7$  yr where  $[C/Fe]$  from our SSP model is over 0.4 dex larger than W09. During this time the enrichment originates only from massive stars (Fig. 11). The stellar yields of the massive star models span 1.7 dex in  $[C/Fe]$  over the initial mass range.

$[C/Fe]$  in the SSP ejecta is very sensitive to the upper limit of the IMF yield range. A decrease of the

upper IMF yield limit from our best value matching W09 of  $M_{\text{ZAMS}} = 100 M_{\odot}$  down to  $M_{\text{ZAMS}} = 30 M_{\odot}$  results in a better agreement with the first value of  $[\text{C}/\text{Fe}] = 0.7$  of W09 (Fig. 13). But later in the evolution  $[\text{C}/\text{Fe}]$  drops by about 0.5 dex below the results of W09. The choice of the upper limit of the IMF as W09 together with the same interpolation of C and Fe with initial mass as W09 could result in a better agreement.  $[\text{N}/\text{Fe}]$ ,  $[\text{O}/\text{Fe}]$  and in particular  $[\text{Si}/\text{Fe}]$  of the yields vary less strongly with initial mass which might explain

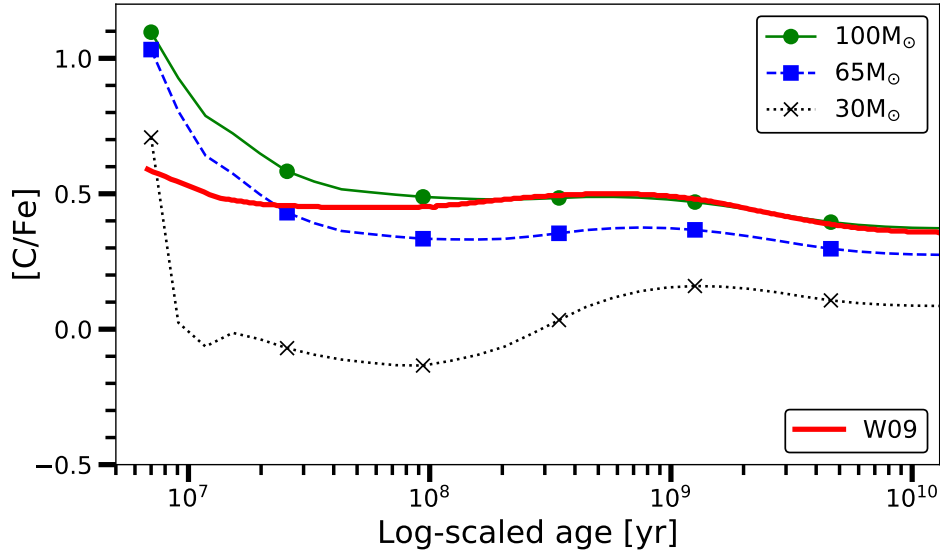


Fig. 13.— Evolution of  $[\text{C}/\text{Fe}]$  for upper boundaries of  $M_{\text{ZAMS}} = 30 M_{\odot}$ ,  $M_{\text{ZAMS}} = 65 M_{\odot}$  and  $M_{\text{ZAMS}} = 100 M_{\odot}$  up to which yields are applied.

the better agreement with W09 (Fig. 12).

To compare the effect of SSP assumptions and yield input we distinguish between the same SSP assumptions but different yield input (Fig. 14) and different SSP assumptions with same yield input (Fig. 9). The total ejecta of AGB stars and massive stars are in better agreement when applying the same chemical evolution assumptions. Early on when AGB stars eject matter there is a larger disagreement in the evolution of C due to different chemical evolution assumptions while at later times is due to different yield input. The evolution of N, O and Si differ the most for different yield input which is likely due to the treatment of fallback in the stellar models. Fe differs stronger with the change in chemical evolution assumptions than with change in yield input. The same SNIa yields are applied in both sets which results in a good agreement when the same chemical evolution assumptions are applied. Overall we find that differences in yield input is more relevant than the differences in the SSP implementation

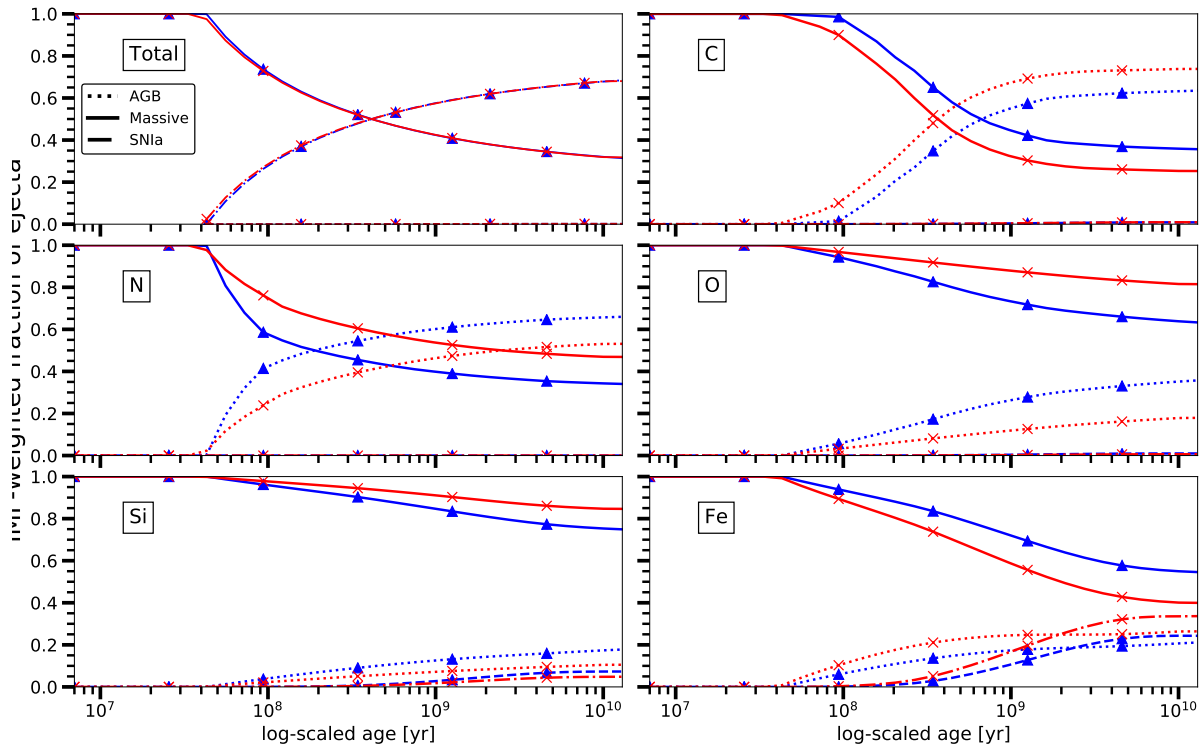


Fig. 14.— Fraction of total mass ejected from AGB, massive star and SNe Ia for a SYGMA SSP at solar metallicity with NuGrid yield (blue, crosses) and yields from M01P98 (red).

#### 4.2. Impact of mass-cut prescriptions

The composition of SSP ejecta depends on the choice of the CCSN prescription and fallback of the massive star models. NuGrid provides stellar yields with two different explosion prescriptions (yield set NuGrid<sub>d</sub>, yield set NuGrid<sub>r</sub>, Table 1) based on the convective-enhanced neutrino-driven engine and we discuss the impact of these prescriptions for SSPs at  $Z = 0.02$  and  $Z = 0.001$  (e.g. Fryer & Young 2007; Fryer et al. 2012, F12). On a short timescale the rapid-convection engine provides enough energy for a successful explosion. The delayed-convection explosion requires longer times to deposit enough energy to explode which results in more fallback and larger remnants for stellar models of  $Z = 0.02$  and  $Z = 0.001$  (Fig. 15). The  $25 M_{\odot}$ ,  $Z = 0.02$  model is an exception to this statement. The remnant mass in the delayed explosion increases with initial mass while the remnant mass for the rapid explosion peaks strongly around  $M_{\text{ZAMS}} = 24 M_{\odot}$ . The latter results in the large remnant mass of  $15.5 M_{\odot}$  for our stellar model with  $M_{\text{ZAMS}} = 25 M_{\odot}$ . According to F12 this stellar model collapses directly into a BH which results the total mass at collapse as the remnant mass (Fig. 15).

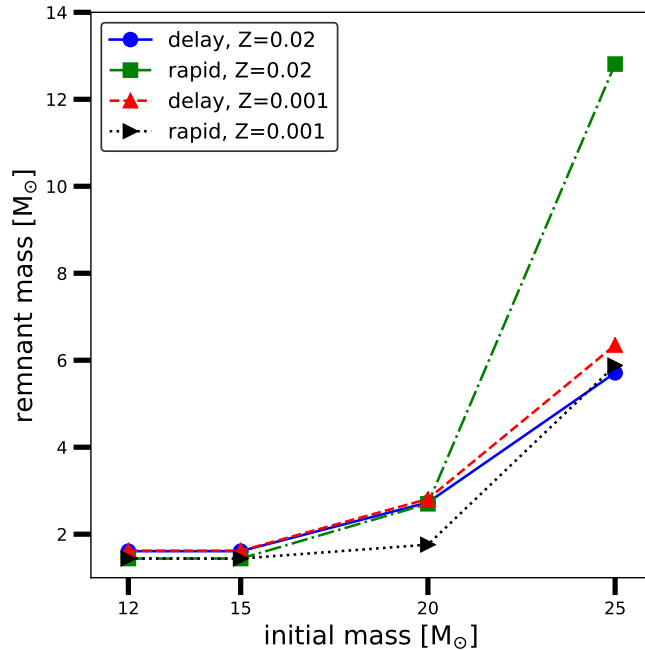


Fig. 15.— Remnant masses based on stellar models of  $Z = 0.02$  and  $Z = 0.001$  from NuGrid and calculated the delayed and rapid explosion prescriptions.

We compare the impact of the two fallback prescriptions on the massive star ejecta of SSPs of  $10^4 M_{\odot}$  for  $Z = 0.02$  and  $Z = 0.001$  (Fig. 16). The SSP ejecta of C, O and Si differ more between the fallback prescriptions at  $Z = 0.02$  than at  $Z = 0.001$  due to the BH formation after the rapid explosion of the stellar

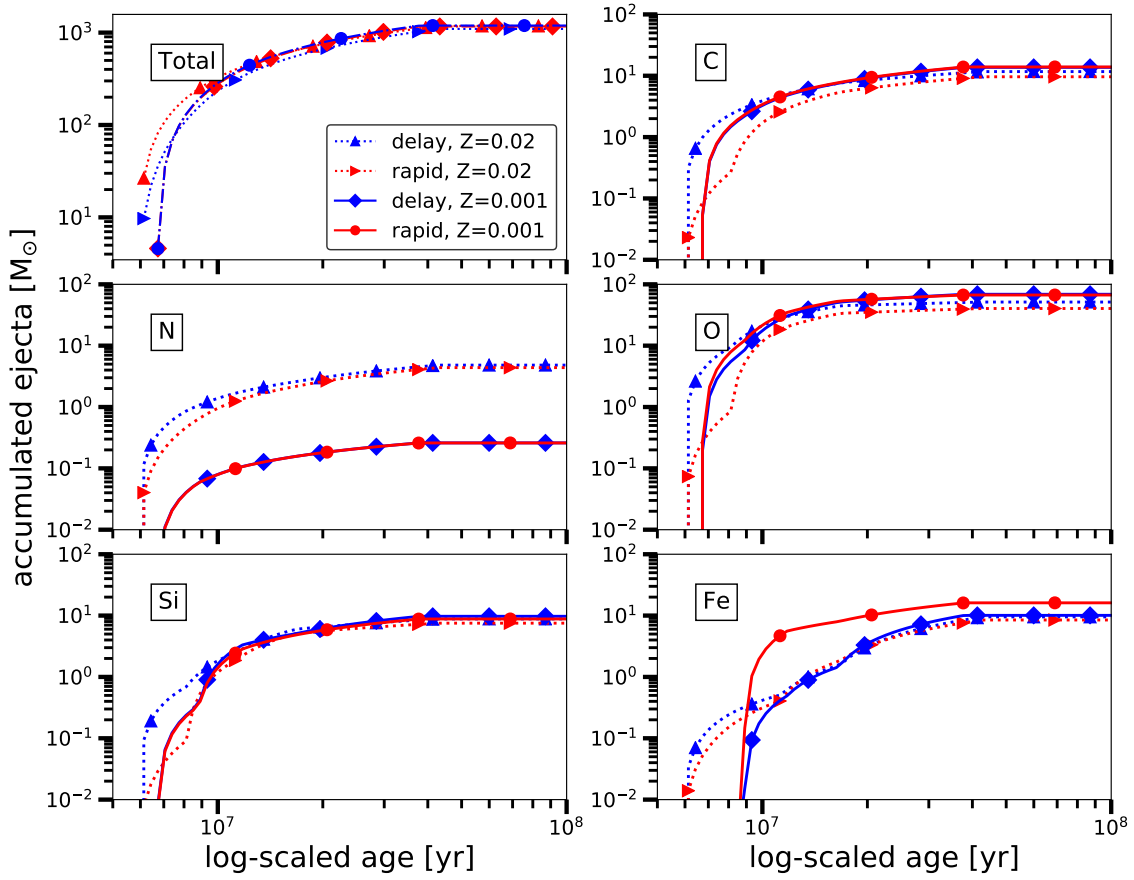


Fig. 16.— Accumulated ejecta of massive stars of NuGrid yields at  $Z = 0.02$  and  $Z = 0.001$  computed with the delayed and rapid CCSN fallback prescription.

model with  $M_{\text{ZAMS}} = 25 M_{\odot}$  at  $Z = 0.001$ . This prevents the ejection of the Si, O and C shell. Similar amounts of Fe fall back onto the remnant with both explosion prescriptions due to the deep location of the Fe core. The SSP ejecta of Fe show only smaller differences. The ejection of elements of the SSP at  $Z = 0.001$  agree well except for Fe. Small amounts of fallback in the rapid explosion of the stellar model with  $M_{\text{ZAMS}} = 20 M_{\odot}$  and a sufficient large Fe core result in the ejection of a thin layer of the Fe core which boosts the amount of Fe SSP ejecta. Within the first  $1.3 \times 10^7$  yr ten times more Fe is ejected with the rapid explosion compared to the delayed explosion. The expected range of explosion delay times (F12) could lead to large variations in Fe enrichment in the early universe.

The rapid explosion models match better the observed gap between NS and BH remnants than the delayed models even though the gap might be sparsely populated (references in F12). Delayed explosions produce more fallback BHs, in particular at low mass and yield a larger fraction of low-mass BHs formed with a SN explosion. The latter can explain the observed BH systems which indicate a natal kick (F12). Fallback is also relevant to produce the weak supernova (Valenti et al. 2009) which are believed to be observed (F12). While the yield sets with the delayed and rapid CCSN explosion prescription are valid to use we recommend yields with the delayed explosion prescription in chemical evolution models. F12 argues that both extremes might be necessary to explain all SN observations. We combine yields of the delayed and rapid explosions to take into account explosions on short and long timescale and provide a yield table which contains as a mixture half of the yields of each prescription (yield set NuGrid<sub>d/r/m</sub>, Table 1).

## 5. Summary and Conclusions

The SYGMA module provides the chemical ejecta and stellar feedback of simple stellar populations for hydrodynamical simulations and semi-analytical models of galaxies. We presented the model assumptions and capabilities which include a variety of SNIa delay-time distributions and IMFs to study their impact on the element enrichment. The IMF type and initial mass range can be specified to take into account BH formation and top-heavy IMFs as expected for PopIII stars.

Modeling the ejecta of NS mergers and CCSN neutrino-driven winds allow to track the r-process enrichment in the early Universe besides the typical AGB, massive star and SNIa ejecta modeled in `starburst99` and W09. The individual contribution from each source are tracked and can be analyzed.

The application of NuGrid yields allow to use AGB yields, massive star yields and CCSN contributions based on the same codes and nuclear reaction rates. Large, unquantifiable uncertainties which origin from the application of different AGB and massive star yield sets can be avoided. Our module models stellar ejecta and feedback of AGB stars *and* massive stars in contrast to `starburst99`. NuGrid yields are not based on synthetic stellar models such as the AGB yields in `starburst99`, but instead all isotopes are calculated from post-processing of stellar evolution models.

SYGMA tracks an arbitrary number of element and isotopes up to Bi as provided by NuGrid while SSP models such as of W09 trace only a few elements. NuGrid yield tables are available in a large yield library which includes yields from MHD jets, hypernova and NS mergers while other tables are added on request.

Yield tables with updated input physics as part of future NuGrid efforts will be directly available in SYGMA.

Stellar feedback from CCSNe is consistent with the underlying explosion models applied in NuGrid yields while W09 adopt a constant energy release. Stellar luminosities in energy bands are calculated from time-dependent synthetic spectra of NuGrid stellar models and as such consistent with NuGrid yield input.

An online interface can be used to simulate, analyze and extract the ejecta SSP ejecta in tabulated form for choices of chemical evolution parameters (Appendix A). Access to the web interface, documentation, interactive examples are available at <http://nugrid.github.io/NuPyCEE>. SYGMA is the basic building block of NuGrids chemical evolution framework NuPyCEE.

SYGMA is used to spawn the SSPs for the galaxy code OMEGA which is applied in a variety of galactic chemical evolution studies (Côté et al. 2016, 2017a,b). It is used to investigate the impact of chemical evolution assumptions and nuclear physics uncertainties through the JINA-NuGrid galactic chemical evolution pipeline (Côté et al. 2017c).

The SSP ejecta based on the NuGrid yields and the combined yields of P98 and M01 are compared at solar and at low metallicity. The differences for C and N ejecta are due to massive and super-AGB stars and are the largest at low metallicity with a factor of 3.5 and 4.8. This is due to the complete stellar models of NuGrid which include the TP-AGB stage and HBB in the most massive AGB models. O, Si and Fe in the SSP ejecta vary within a factor of  $\approx 2$  and the largest differences are found at solar metallicity due to the different CCSN fallback treatments.

The functionality of the module was verified through a comparison with W09 in which we apply their yields. The final accumulated ejecta are well in agreement in both works and the largest differences in the fraction of ejecta of N and Fe from massive stars is 10%.

We have analyzed the impact of CCSN fallback prescriptions of massive stellar models on the ejecta composition of SSPs at  $Z = 0.02$  and  $Z = 0.001$ . At the latter metallicity we find the largest variations for C, O and Si of about a factor of ten in the first  $10^7$  yr. The total ejecta of these elements differ by less than a factor two. The largest difference of the total ejecta between the fallback prescriptions is for Fe with a factor 1.6.

We are grateful to Else Starckenburg and Kim Venn for their valuable discussion about the concept of the SYGMA module. We are thankful to Luke Siemens and Jericho O’Connell for building the IPython widgets for SYGMA. We acknowledge Adam Paul for his contributions to the NS merger implementation. NuGrid acknowledges significant support from NSF grant PHY-1430152 (JINA Center for the Evolution of the Elements). BC was supported by the FRQNT (Quebec, Canada) postdoctoral fellowship program. We acknowledge the Canadian Advanced Network for Astronomical Research cloud service which hosts the SYGMA web interface. CR received funding from the European Research Council under the European Union’s Seventh Framework Programme (FP/2007-2013)/ERC Grant Agreement n. 306901.

## REFERENCES

- Abbott, D. C. 1978, *ApJ*, 225, 893
- Arnett, D. 1996, *Supernovae and Nucleosynthesis*
- Arnett, W. D., Bahcall, J. N., Kirshner, R. P., & Woosley, S. E. 1989, *ARA&A*, 27, 629
- Arnould, M., Goriely, S., & Takahashi, K. 2007, *Phys. Rep.*, 450, 97
- Audouze, J., & Tinsley, B. M. 1976, *ARA&A*, 14, 43
- Bolton, C. T. 2000, *Physics Today*, 53, 48
- Castelli, F., & Kurucz, R. L. 2004, *ArXiv Astrophysics e-prints*
- Chabrier, G. 2003, *PASP*, 115, 763
- Côté, B., Belczynski, K., Fryer, C. L., Ritter, C., Paul, A., Wehmeyer, B., & O’Shea, B. W. 2017a, *ApJ*, 836, 230
- Côté, B., Martel, H., & Drissen, L. 2015, *ApJ*, 802, 123
- Côté, B., O’Shea, B. W., Ritter, C., Herwig, F., & Venn, K. A. 2017b, *ApJ*, 835, 128
- Côté, B., Ritter, C., Herwig, F., O’Shea, B. W., Pignatari, M., Silvia, D., Jones, S., & Fryer, C. L. 2017c, in *14th International Symposium on Nuclei in the Cosmos (NIC2016)*, ed. S. Kubono, T. Kajino, S. Nishimura, T. Isobe, S. Nagataki, T. Shima, & Y. Takeda, 020203
- Côté, B., Ritter, C., O’Shea, B. W., Herwig, F., Pignatari, M., Jones, S., & Fryer, C. L. 2016, *ApJ*, 824, 82
- Côté, B., Silvia, D., O’Shea, B. W., Smith, B., & Wise, J. H. 2017d, *ArXiv e-prints*
- Côté, B., et al. 2017e, *ArXiv e-prints*
- Cristallo, S., Straniero, O., Piersanti, L., & Gobrecht, D. 2015, *ApJS*, 219, 40
- Dahlen, T., et al. 2004, *ApJ*, 613, 189
- Doherty, C. L., Gil-Pons, P., Siess, L., & Lattanzio, J. C. 2017, *ArXiv e-prints*
- Doherty, C. L., Gil-Pons, P., Siess, L., Lattanzio, J. C., & Lau, H. H. B. 2015, *MNRAS*, 446, 2599
- Dominik, M., Belczynski, K., Fryer, C., Holz, D. E., Berti, E., Bulik, T., Mandel, I., & O’Shaughnessy, R. 2012, *ApJ*, 759, 52
- Ferrarotti, A. S., & Gail, H.-P. 2006, *A&A*, 447, 553
- Fryer, C. L., Belczynski, K., Wiktorowicz, G., Dominik, M., Kalogera, V., & Holz, D. E. 2012, *ApJ*, 749, 91

- Fryer, C. L., & Young, P. A. 2007, *ApJ*, 659, 1438
- Gibson, B. K. 2002, in *IAU Symposium*, Vol. 187, *Cosmic Chemical Evolution*, ed. K. Nomoto & J. W. Truran, 159–163
- Heger, A., & Woosley, S. E. 2010, *ApJ*, 724, 341
- Herwig, F. 2005, *Annual Review of Astronomy and Astrophysics*, 43, 435
- Hopkins, P. F., Quataert, E., & Murray, N. 2012, *MNRAS*, 421, 3522
- Husser, T.-O., Wende-von Berg, S., Dreizler, S., Homeier, D., Reiners, A., Barman, T., & Hauschildt, P. H. 2013, *A&A*, 553, A6
- Iwamoto, K., Brachwitz, F., Nomoto, K., Kishimoto, N., Umeda, H., Hix, W. R., & Thielemann, F.-K. 1999, *ApJS*, 125, 439
- Jones, S., Ritter, C., Herwig, F., Fryer, C., Pignatari, M., Bertolli, M. G., & Paxton, B. 2016, *MNRAS*, 455, 3848
- Karakas, A. I. 2011, in *Astronomical Society of the Pacific Conference Series*, Vol. 445, *Why Galaxies Care about AGB Stars II: Shining Examples and Common Inhabitants*, ed. F. Kerschbaum, T. Lebzelter, & R. F. Wing, 3
- Karakas, A. I., Campbell, S. W., & Stancliffe, R. J. 2010, *ApJ*, 713, 374
- Kobayashi, C., Umeda, H., Nomoto, K., Tominaga, N., & Ohkubo, T. 2006, *ApJ*, 653, 1145
- Kroupa, P. 2001, *MNRAS*, 322, 231
- Kroupa, P., Weidner, C., Pflamm-Altenburg, J., Thies, I., Dabringhausen, J., Marks, M., & Maschberger, T. 2013, in *Planets, Stars and Stellar Systems. Volume 5: Galactic Structure and Stellar Populations*, ed. T. D. Oswalt & G. Gilmore, 115
- Lattanzio, J., Frost, C., Cannon, R., & Wood, P. R. 1996, *Mem. Soc. Astron. Italiana*, 67, 729
- Leitherer, C., Robert, C., & Drissen, L. 1992, *ApJ*, 401, 596
- Leitherer, C., et al. 1999, *ApJS*, 123, 3
- Mannucci, F., Della Valle, M., & Panagia, N. 2006, *MNRAS*, 370, 773
- Maoz, D., & Mannucci, F. 2012, *PASA*, 29, 447
- Marigo, P. 2001a, *A&A*, 370, 194
- . 2001b, *A&A*, 370, 194
- Nishimura, N., Takiwaki, T., & Thielemann, F.-K. 2015, *ApJ*, 810, 109

- Nomoto, K., Kobayashi, C., & Tominaga, N. 2013, *ARA&A*, 51, 457
- Pagel, B. E. J. 2009, *Nucleosynthesis and Chemical Evolution of Galaxies* (Cambridge University Press)
- Pignatari, M., et al. 2016, *ApJS*, 225, 24
- Poelarends, A. J. T., Herwig, F., Langer, N., & Heger, A. 2008, *apj*, 675, 614
- Portinari, L., Chiosi, C., & Bressan, A. 1998, *A&A*, 334, 505
- Ritter, C., Andrassy, R., Côté, B., Herwig, F., Woodward, P. R., Pignatari, M., & Jones, S. 2017a, *ArXiv e-prints*
- Ritter, C., Herwig, F., Jones, S., Pignatari, M., Fryer, C., & Hirschi, R. 2017b, *ArXiv e-prints*
- Romano, D., Karakas, A. I., Tosi, M., & Matteucci, F. 2010, *A&A*, 522, A32
- Rosswog, S., Korobkin, O., Arcones, A., Thielemann, F.-K., & Piran, T. 2014, *MNRAS*, 439, 744
- Salpeter, E. E. 1955, *ApJ*, 121, 161
- Schneider, R., Valiante, R., Ventura, P., dell’Agli, F., Di Criscienzo, M., Hirashita, H., & Kemper, F. 2014, *MNRAS*, 442, 1440
- Seitzzahl, I. R., et al. 2013, *MNRAS*, 429, 1156
- Thielemann, F.-K., Nomoto, K., & Yokoi, K. 1986, *Astronomy and Astrophysics*, 158, 17
- Thielemann, F.-K., et al. 2003, in *From Twilight to Highlight: The Physics of Supernovae*, ed. W. Hillebrandt & B. Leibundgut, 331
- Timmes, F. X., Woosley, S. E., & Weaver, T. A. 1995, *APJS*, 98, 617
- Valenti, S., et al. 2009, *Nature*, 459, 674
- Wiersma, R. P. C., Schaye, J., Theuns, T., Dalla Vecchia, C., & Tornatore, L. 2009, *Monthly Notices of the Royal Astronomical Society*, 399, 574
- Woosley, S. E., Heger, A., & Weaver, T. A. 2002, *Rev. Mod. Phys.*, 74, 1015
- Woosley, S. E., & Weaver, T. A. 1995, *APJS*, 101, 181+
- Yungelson, L. R. 2005, in *American Institute of Physics Conference Series*, Vol. 797, *Interacting Binaries: Accretion, Evolution, and Outcomes*, ed. L. Burderi, L. A. Antonelli, F. D’Antona, T. di Salvo, G. L. Israel, L. Piersanti, A. Tornambè, & O. Straniero, 1–10

### A. Online availability

The SYGMA web interface allows to simulate, analyse, and extract SSP ejecta which includes all stable elements and many isotopes up to Bi. We introduce the yield sets and parameters which are available within the web interface. Yields for AGB stars and massive stars can be selected from the NuGrid sets NuGrid<sub>d/r/m</sub> (Table 1) SNIa yields are from Thielemann et al. (2003) and Pop III yields are from Heger & Woosley (2010). The available metallicities are  $Z = 0.02, 0.01, 0.006, 0.001$  and  $0.0001, 0$ . Yields are applied in the initial mass range from  $1 M_{\odot}$  to  $30 M_{\odot}$ . Chemical evolution parameters such as IMF and SNIa DTD can be set.

SSP ejecta can be extracted in the form of tables which contain for each time step the fraction of elements and isotopes of choice. The ejecta of each element or isotope is normalized to the total mass of the SSP. As an example parts of a table which contains the normalized mass of elements ejected over  $10^{10}$  yr by a SSP of  $10^4 M_{\odot}$  at  $Z = 0.02$  is presented in Table 3.

Age [yr]	C	N	O	Fe	Sr	Ba	M_tot [Msun]
0.000E+00	3.466E-03	1.063E-03	9.650E-03	1.438E-03	6.072E-08	1.813E-08	1.000E+04
1.000E+07	7.848E-04	2.770E-04	4.412E-03	8.351E-05	2.715E-08	1.425E-09	6.557E+02
1.269E+07	1.120E-03	3.859E-04	6.546E-03	1.866E-04	4.197E-08	2.014E-09	9.426E+02
				.....			
7.880E+09	6.301E-03	2.697E-03	1.508E-02	2.505E-03	1.391E-05	3.973E-06	7.067E+03
1.000E+10	6.304E-03	2.697E-03	1.509E-02	2.552E-03	1.391E-05	3.973E-06	7.068E+03

Table 3: Table with time evolution of the ejected elements extracted with the SYGMA web interface.

The SYGMA code and the yield library can be accessed via <http://nugrid.github.io/NuPyCEE>. We provide an online documentation based on SPHINX<sup>2</sup>, guides and teaching material in form of Jupyter notebooks. SYGMA web interface is accessible through the NuPyCEE web page and hosted on NuGrid’s Web Exploration of NuGrid Datasets: Interactive (WENDI) platform at <http://wendi.nugridstars.org>. Access to the figures of this work are provided through WENDI. NuGrid’s stellar and nucleosynthesis data sets are available at <http://nugridstars.org/data-and-software/yields/set-1> and can be analyzed with WENDI.

---

<sup>2</sup><http://www.sphinx-doc.org>